ISSN 0020-1685, Inorganic Materials, 2019, Vol. 55, No. 7, pp. 692–697. © Pleiades Publishing, Ltd., 2019.
Russian Text © The Author(s), 2019, published in Neorganicheskie Materialy, 2019, Vol. 55, No. 7, pp. 738–743.

Ordered Defect Lattice in Lithium Niobate Crystals

L. A. Aleshina[a], O. V. Sidorova[a], A. V. Kadetova[a], N. V. Sidorov[b, *], N. A. Teplyakova[b], and M. N. Palatnikov[b]

[a] *Petrozavodsk State University, Universitetskaya ul. 10a, Petrozavodsk, 185910 Karelia, Russia*

[b] *Tananaev Institute of Chemistry and Technology of Rare Elements and Mineral Raw Materials (Separate Division), Kola Scientific Center (Federal Research Center), Russian Academy of Sciences, Akademgorodok 26a, Apatity, Murmansk oblast, 184209 Russia*

**e-mail: sidorov@chemy.kolasc.net.ru*

Received July 3, 2018; revised February 5, 2019; accepted February 13, 2019

Abstract—Nominally undoped and doped $LiNbO_3$ crystals have been studied using full-profile analysis of X-ray diffraction data and Raman spectroscopy. The X-ray diffraction patterns and Raman spectra of the crystals contain weak superstructure lines forbidden for space group *R*3*c*. The observed superstructure lines are not reflections from a second phase. The intensity distribution and position of the additional reflections are essentially independent of nonstoichiometry and dopant concentration. The additional lines in the Raman spectra and X-ray diffraction patterns of the crystals can result from the formation of an ordered hexagonal defect superstructure sublattice with a doubled *a* cell parameter relative to the fundamental unit cell.

Keywords: lithium niobate single crystal, full-profile analysis of X-ray diffraction data, Raman spectroscopy, superstructure

DOI: 10.1134/S0020168519070033

INTRODUCTION

As shown in extensive studies [1–9], Raman spectra of real lithium niobate ($LiNbO_3$) crystals of various compositions contain considerably more lines than is allowed by the selection rules for a structure with C_{3v}^6 (*R*3*c*) space group symmetry and two formula units per unit cell. In addition to lines corresponding to fundamental lattice modes and second-order scattering, Raman spectra of nominally undoped $LiNbO_3$ crystals (with different Li/Nb ratios) and doped ones in different scattering geometries show weak lines at frequencies of 85, 92, 100, 108, 120, 187, 200, 305, 311, 331, 412, 440, 477, 535, 605, 668, 694, 739, 743, 773, 825, and 890 cm^{-1}, which are referred to as superstructure ("extra") lines [1–5]. The origin of the "extra" lines is rather difficult to interpret: a considerable number of them have not been assigned to particular scattering processes. The nature of the "extra" lines is currently the subject of intense controversy in the literature [1–9], and they seem to arise from lattice defects [10–12]. The frequencies of the "extra" lines differ from the frequencies of fundamental modes, their intensity is almost two orders of magnitude lower, and the number of these lines is comparable to that of the lines corresponding to fundamental lattice modes.

There are grounds to believe that some of the "extra" lines in the Raman spectrum of $LiNbO_3$ crystals are due to the formation of an ordered defect superstructure sublattice, which has its own Raman spectrum. This is possible because lithium niobate is a nonstoichiometric phase of variable composition with a broad homogeneity range in its phase diagram and exhibits a rich defect chemistry [1, 11, 12]. In connection with this, it is of interest to perform an in-depth X-ray diffraction study of the structural state of $LiNbO_3$ crystals with different compositions.

In this paper, we report full-profile X-ray diffraction and Raman spectroscopy studies of a nominally undoped, nearly stoichiometric lithium niobate ($LiNbO_{3\ stoich}$) crystal; a congruent lithium niobate ($LiNbO_{3\ congr}$) crystal; and doped $LiNbO_3$ crystals: $LiNbO_3$:Er (0.062, 0.84, 2.19, 2.48, 2.66, and 2.67 mol % Er_2O_3), $LiNbO_3$:Zn (6.52 mol % ZnO), and $LiNbO_3$:Tb (3 mol % Tb_2O_3).

EXPERIMENTAL

A $LiNbO_{3\ congr}$ single crystal was grown by a standard Czochralski process [12, 13] in air from a melt of congruent composition. A $LiNbO_{3\ stoich}$ single crystal was grown from a melt containing 58.6 mol % Li_2O, using a growth charge prepared as described elsewhere [14]. The concentration of foreign impurities in the growth charge did not exceed 5×10^{-4} wt %. A $LiNbO_3$:Zn crystal containing 6.52 mol % ZnO was prepared via homogeneous doping of Nb_2O_5 as a precursor [15,

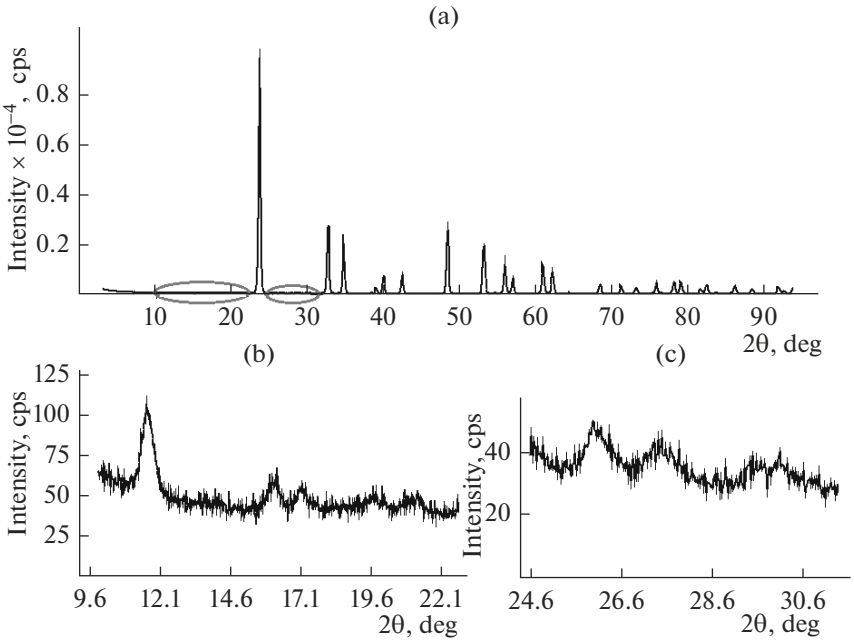

Fig. 1. (a) X-ray diffraction pattern of the $LiNbO_3$:Er (0.062 mol % Er_2O_3) crystal, with the ranges of additional reflections indicated (shown in Figs. 1b and 1c).

16]. $LiNbO_3$:Er (0.062, 0.84, 2.19, 2.48, 2.66, and 2.67 mol % Er_2O_3) and $LiNbO_3$:Tb (3.0 mol % Tb_2O_3) crystals were prepared by a direct doping method, that is, by adding appropriate metal oxides to a granulated lithium niobate growth charge and mixing before melting in a crucible. The procedures used to prepare the growth charge and grow crystals with various compositions were described in detail previously [12–17].

X-ray diffraction patterns were collected in the scattering angle range $2\theta = 5°$ to 145° on a DRON-6 diffractometer (CuK_α radiation, incident-beam pyrolytic graphite monochromator). For automatic indexing and unit cell refinement, we used the Ind program in a PDWin program suite (Burevestnik Innovation Center, JSC), which implements the Ito method, based on mathematical relations in the reciprocal lattice. Raman spectra were excited by the 514.5-nm argon laser line (Spectra Physics, Model 2018-RM) and measured with a Horiba Jobin Yvon T64000 spectrograph using a confocal microscope. Samples for the Raman measurements were cut from the crystals and had the form of rectangular parallelepipeds (~7 × 6 × 5 mm in dimensions) whose edges were parallel to the *X*, *Y*, and *Z* crystal-physical axes (where *Z* is the polar axis of the crystals). The faces of the parallelepipeds were thoroughly polished.

RESULTS AND DISCUSSION

Figure 1 shows X-ray diffraction patterns of the $LiNbO_3$:Er (0.062 mol % Er_2O_3), $LiNbO_3$:Zn (6.52 mol % ZnO), and $LiNbO_3$:Tb (3 mol % Tb_2O_3) crystals, where the regions of additional reflections are indicated. Figure 2 shows the first region of weak additional reflections for the stoichiometric and congruent lithium niobate crystals, as well as for the $LiNbO_3$:Zn (6.52 mol % ZnO) and $LiNbO_3$:Tb (3 mol % Tb_2O_3) doped crystals. It is seen from Figs. 1 and 2 that all of the crystals studied have similar X-ray diffraction patterns. Note that the first reflection corresponding to the *R3c* $LiNbO_3$ phase appears in the X-ray diffraction patterns at a scattering angle of 23.7° and has the highest intensity. Moreover, it is seen that all of the X-ray diffraction patterns obtained show not only the main reflections from the $LiNbO_3$ phase but also additional lines at scattering angles in the ranges from 11° to 22° and from 25.3° to 31°. The strongest reflection is located at a scattering angle of ~11.8°. Table 1 presents calculated scattering angles and interplanar spacings for the additional lines in the X-ray diffraction patterns of the $LiNbO_{3\ congr}$, $LiNbO_{3\ stoich}$, and $LiNbO_3$:Er (0.062, 0.84, 2.19, 2.48, 2.66, 2.67 mol % Er_2O_3) crystals.

It is seen in Fig. 2 that the additional lines are present in not only X-ray diffraction patterns of the doped crystals, which have the most disordered cation sublattice, but also in the X-ray diffraction patterns of the $LiNbO_{3\ stoich}$ and $LiNbO_{3\ congr}$ crystals. This finding indicates that the lines in question are unrelated to doping. It should also be noted that, in all of the samples the intensity distribution and the position of the additional reflections are independent of dopant concentration. The same refers to the Raman spectra of the crystals: the frequencies and intensities of many "extra" lines that have not been assigned to particular

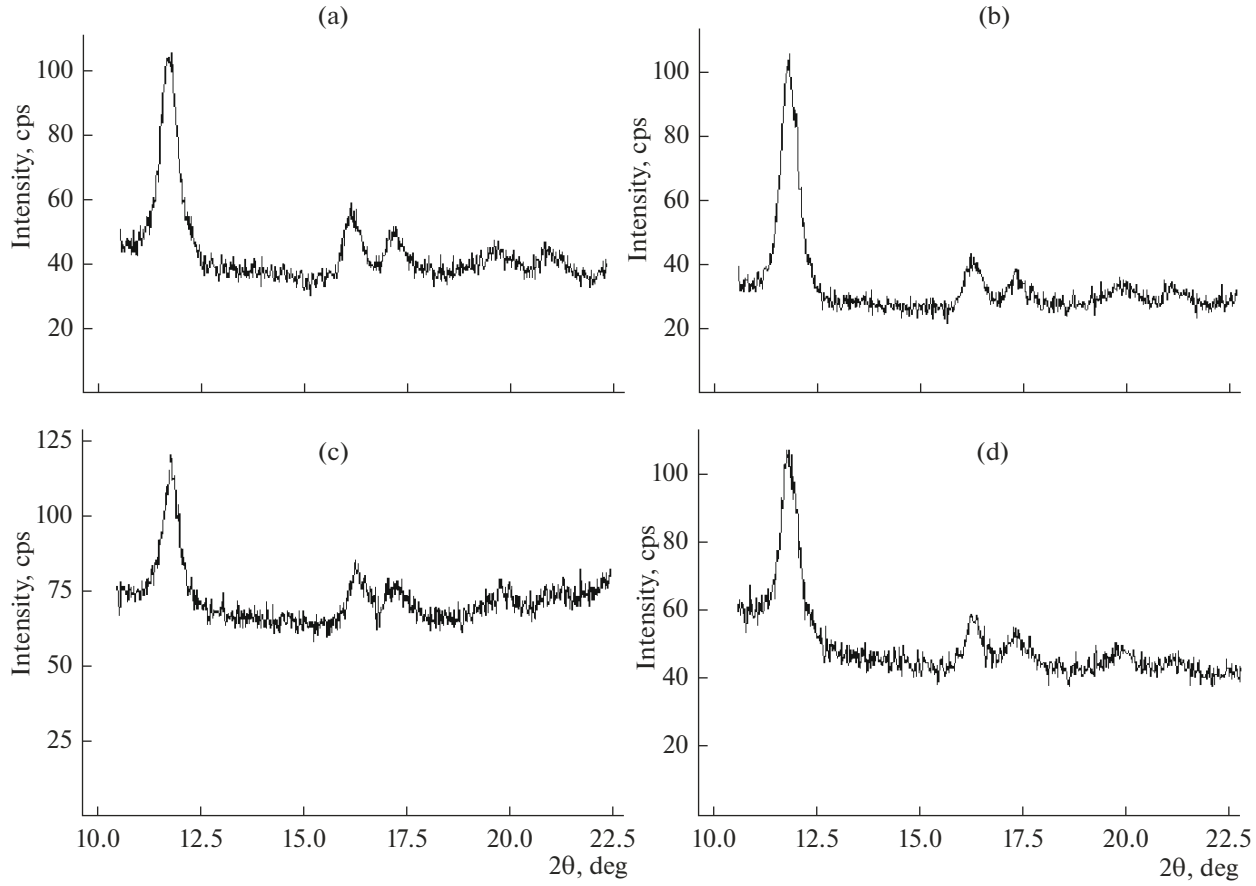

Fig. 2. Additional reflections in the X-ray diffraction patterns of the (a) stoichiometric $LiNbO_3$, (b) congruent $LiNbO_3$, (c) $LiNbO_3$:Zn (6.52 mol % ZnO), and (d) $LiNbO_3$:Tb (3 mol % Tb_2O_3) crystals.

scattering processes are independent of the composition of the nonstoichiometric crystals [1–5]. At the same time, the Raman spectrum of the stoichiometric lithium niobate crystal, which has high structural perfection, is free of "extra" lines. As an example, Fig. 3 shows the Raman spectrum of the congruent lithium niobate single crystal in the $Y(ZZ)\bar{Y}$ scattering geometry (the "extra" lines are marked by arrows).

We carried out a qualitative phase analysis using the Inorganic Crystal Structure Database (ICSD). The additional lines observed in the X-ray diffraction patterns of our samples were found to differ in position from all lines of possible phases.

All of the above led us to assume that the observed "extra" lines were not reflections from a second phase, but more likely resulted from the formation of an ordered superstructure in the nonstoichiometric lithium niobate samples. To verify this assumption, the entire X-ray diffraction patterns of the crystals were indexed, together with the additional lines. The additional reflections indicated above could not be indexed in hexagonal symmetry with lattice parameters $a = 5.14941$ and $c = 13.86186$ Å (Table 2), nor was it possible with lattice parameters $a' = a$ and $c' = 2c$. Therefore, there are no displacements of atoms along the c axis that might cause the c cell parameter to double. At the same time, indexing in hexagonal symmetry with a doubled a cell parameter ($a' = 2a$ and $c' = c$) allowed the weak additional lines to be indexed. Table 2 presents typical indexing results for the X-ray diffraction pattern of the $LiNbO_3$:Er (0.062 mol % Er_2O_3) crystal. In Table 2, first- and second-order reflections from the same system of planes are denoted by the same symbols. The 226 line (second-order reflection from the (113) planes) falls in the region of the overlapping reflections 330 and 421. It is worth noting that, using direct (automatic) indexing in hexagonal symmetry and making assumptions about fundamental lines, but without assumptions about lattice parameters, we obtained the same result: $a' = 2a$ and $c' = c$. After refinement of the lattice parameters obtained as a result of automatic indexing, the indexing figure of merit M_{20}, introduced by de Wolff, was 22, suggesting high reliability of the results obtained. Analysis of the Miller indices indicates that all of the weak lines are first-order reflections from planes of the fundamental lattice.

Table 1. Scattering angles (2θ, deg) of the additional reflections from and the corresponding calculated interplanar spacings (d, Å) in the $LiNbO_{3\ stoich}$, $LiNbO_{3\ congr}$, and $LiNbO_3$:Er crystals

$LiNbO_{3\ stoich}$	2θ	11.76	16.20	17.23	19.63	21.07	26.06	27.58	29.97		
	d	7.53	5.47	5.15	4.52	4.22	3.42	3.23	2.98		
$LiNbO_{3\ congr}$	2θ	11.82	16.26	17.35	19.87	21.09	26.22	27.55	30.07		
	d	7.49	5.45	5.11	4.47	4.21	3.39	3.24	2.97		
0.062*	2θ	11.76	16.18	17.20	19.69	21.14	26.08	27.51	29.55	30.15	
	d	7.52	5.48	5.16	4.51	4.20	3.42	3.24	3.02	2.96	
0.84*	2θ	11.82	16.33	17.31	19.85	21.03	26.12	27.6	29.6	30.3	
	d	7.49	5.43	5.12	4.47	4.22	3.42	3.23	3.01	2.95	
2.19*	2θ	11.88	16.23	17.25	19.8	21.00	26.1	27.26	27.83	29.60	30.17
	d	7.45	5.46	5.14	4.48	4.22	3.41	3.27	3.21	3.02	2.96
2.48*	2θ	11.78	16.24	17.23	19.73	21.21	26.04	27.53	29.43	30.07	
	d	7.51	5.46	5.15	4.50	4.19	3.42	3.24	3.03	2.97	
2.66*	2θ	11.80	16.18	17.18	19.67	21.0	26.00–26.39	27.12–27.65	28.56	29.41	30.06
	d	7.50	5.47	5.16	4.51	4.23	3.43 3.38	3.28 3.23	3.12	3.04	2.97
2.67*	2θ	12.12	16.32	17.23	19.81	21.13	26.18	27.79	30.0		
	d	7.30	5.43	5.14	4.82	4.21	3.40	3.21	2.98		

* mol % Er.

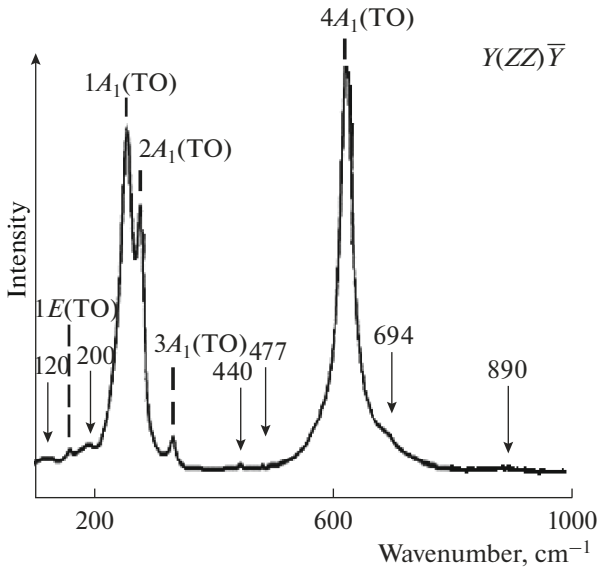

Fig. 3. Raman spectrum of the congruent lithium niobate single crystal in the $Y(ZZ)\overline{Y}$ scattering geometry. The "extra" lines are marked by arrows. The line corresponding to the $1E$(TO) fundamental mode (ν = 150 cm^{-1}) is seen in the spectrum as a result of uncertainties in our polarization measurements and the photorefractive effect.

Thus, the weak reflections observed in the X-ray diffraction patterns of the doped and undoped lithium niobate crystals are superstructure lines, forbidden for space group $R3c$ of a lattice with parameters a = 5.1494 Å and c = 13.862 Å. The formation of the superstructure leads to a doubled a cell parameter, that is, to a hexagonal lattice having a four times larger unit-cell volume. It is quite possible that a considerable number of the numerous weak "extra" lines observed by many researchers in Raman spectra correspond to the spectrum of fundamental vibrations of this hexagonal superstructure lattice.

CONCLUSIONS

Full-profile analysis of X-ray diffraction data and Raman spectroscopy have been used to study congruent and nearly stoichiometric $LiNbO_3$ crystals, as well as doped lithium niobate crystals grown from different charges: $LiNbO_3$:Er (0.062, 0.84, 2.19, 2.48, 2.66, and 2.67 mol % Er_2O_3), $LiNbO_3$:Zn (6.52 mol % ZnO), and $LiNbO_3$:Tb (3.0 mol % Tb_2O_3). The X-ray diffraction patterns of all the crystals contain additional lines forbidden for space group $R3c$ of a lattice with

Table 2. Indexing results for the X-ray diffraction pattern of the $LiNbO_3$:Er (0.062 mol % Er_2O_3) crystal (columns 2–6 refer to the *R*3*c* structure, columns 8–13 refer to a lattice with a superstructure, and columns 1 and 7 present observed values)

Q_{obs}	Q_{calc}	$\|\Delta Q\|$	*h*	*k*	*l*	Q_{obs}	Q_{calc}	$\|\Delta Q\|$	*h*	*k*	*l*	
a = 5.1494 Å, c =13.862 Å, V = 318.3 Å^3						a = 10.301 Å, c = 13.876 Å, V = 1277 Å^3						
1	2	3	4	5	6	7	8	9	10	11	12	13
176.6						176.6	177.4	0.8	1	0	1	*
333.1						333.1	333.2	0.05	1	0	2	◆
376.1						376.1	376.4	0.3	1	1	0	~
492.1						492.1	501.9	9.8	2	0	0	●
566.1						566.1	553.8	12.4	2	0	1	○
706.9	711.0	4.1	1	0	2	706.9	709.6	2.7	2	0	2	*
856.9						856.9	843.8	13.1	1	1	3	
951.8						951.8	956.3	4.5	1	0	4	∨
1094.2						1094.2	1086.0	8.2	2	1	2	+
1138.1						1138.1	1129.2	8.9	3	0	0	◇
1331.1	1335.5	4.4	1	0	4	1331.1	1332.7	1.6	2	0	4	◆
1504.4	1508.5	4.0	1	1	0	1504.4	1505.6	1.2	2	2	0	~
1869.8	1873.5	3.7	0	0	6	1869.8	1869.5	0.3	0	0	6	
1973.4	1976.8	3.5	1	1	3	1973.4	1973.0	0.4	4	0	0	●
2215.8	2219.4	3.7	2	0	2	2215.8	2215.2	0.6	4	0	2	○
2840.5	2843.9	3.4	2	0	4	2840.5	2842.5	2.0	4	0	4	
3379.8	3381.9	2.1	1	1	6	3379.8	3375.1	4.8	3	3	0	
3569.8	3571.8	2.0	2	1	1	3569.8	3564.9	4.9	4	2	1	
3725.3	3727.9	2.6	2	1	2	3725.3	3720.7	4.5	4	2	2	
3830.2	3833.5	3.2	1	0	8	3830.2	3825.4	4.8	2	0	8	∨
4349.4	4352.4	3.0	2	1	4	4349.4	4343.9	5.5	4	2	4	+
4523.7	4525.4	1.6	3	0	0	4523.7	4516.8	6.9	6	0	0	◇
4822.5	4820.8	1.7	2	1	5	4822.5	4829.1	6.6	2	2	8	

Q_{obs} is the $10^4/d^2_{obs}$ observed value, where d_{obs} is the observed interplanar spacing; $Q_{calc} = 10^4/d^2_{calc}$, where d_{calc} is the interplanar spacing calculated from the lattice parameters obtained as result of indexing and the Miller indices *hkl*; $|\Delta Q| = 10^4 \Delta d^2$.

parameters a = 5.1494 Å and c = 13.862 Å. The formation of the superstructure leads to a doubled a cell parameter, that is, to a hexagonal lattice having a four times larger unit-cell volume.

A qualitative phase analysis using the ICSD database indicates that the observed "extra" lines are not reflections from a second phase. Additional distortion parameters have been shown to be independent of the nature and concentration of dopant cations. Raman spectra of the nonstoichiometric lithium niobate crystals also show weak "extra" lines, independent of the composition of the crystals.

Thus, the present Raman spectroscopy and full-profile X-ray diffraction data suggest that the nonstoichiometric lithium niobate crystals contain an ordered defect sublattice, which contributes to their Raman spectra and X-ray diffraction patterns in the form of "extra" (superstructure) lines.

REFERENCES

1. Sidorov, N.V., Volk, T.R., Mavrin, B.N., and Kalinnikov, V.T., *Niobat litiya: defekty, fotorefraktsiya, kolebatel'nyi spektr, polyaritony* (Lithium Niobate: Defects, Photorefractive Properties, Vibrational Spectrum, and Polaritons), Moscow: Nauka, 2003.
2. Sidorov, N.V., Palatnikov, M.N., and Kalinnikov, V.T., Raman spectra and features of the structure of lithium niobate crystals, *Opt. Spectrosc.,* 1997, vol. 82, no. 1, pp. 32–38.
3. Sidorov, N.V., Palatnikov, M.N., Serebryakov, Yu.A., Lebedeva, E.L., and Kalinnikov, V.T., Effect of nonstoichiometry on the structure, properties, and Raman spectra of lithium niobate crystals, *Inorg. Mater.,* 1997, vol. 33, no. 4, pp. 419–427.
4. Sidorov, N.V. and Palatnikov, M.N., Raman spectra of lithium niobate crystals heavily doped with zinc and magnesium, *Opt. Spectrosc.,* 2016, vol. 121, no. 6,

pp. 842–850.
https://doi.org/10.1134/S0030400X16120225

5. Gorelik, V.S. and Sverbil', P.P., Raman scattering by longitudinal and transverse optical vibrations in lithium niobate single crystals, *Inorg. Mater.,* 2015, vol. 51, no. 11, pp. 1104–1110.
https://doi.org/10.1134/S0020168515100076
6. Anikiev, A.A. and Umarov, M.F., Quasi-elastic light scattering in congruent lithium niobate crystals, *Opt. Spectrosc.,* 2018, vol. 125, no. 1, pp. 22–27.
https://doi.org/10.1134/S0030400X18070020
7. Surovtsev, N.V., Malinovskii, V.K., Pugachev, A.M., and Shebanin, A.P., The nature of low-frequency Raman scattering in congruent melting crystals of lithium niobate, *Phys. Solid State,* 2003, vol. 45, no. 3, pp. 534–541.
https://doi.org/10.1134/1.1562243
8. Lengyel, K., Peter, A., Kovacs, L., Corradi, G., Palfavi, L., Hebling, J., Unferdorben, M., Dravecz, G., Hajdara, I., Szaller, Zs., and Polgar, K., Growth, defect structure, and THz application of stoichiometric lithium niobate, *Appl. Phys. Rev.,* 2015, vol. 2, pp. 040 601–040 628.
https://doi.org/10.1063/1.4929917
9. Fontana, M.D. and Bourson, P., Microstructure and defects probed by Raman spectroscopy in lithium niobate crystals and devices, *Appl. Phys. Rev.,* 2015, no. 2, paper 04 0602.
https://doi.org/10.1063/1.4929917
10. Maradudin, A.A., *Theoretical and Experimental Aspects of the Effects of Point Defects and Disorder on the Vibrations of Crystals,* New York: Academic, 1966.
11. Abrahams, S.C. and March, P., Defect structure dependence of composition in lithium niobate, *Acta Crystallogr., Sect. B: Struct. Sci.,* 1986, vol. 42, no. 2, pp. 61–68.
https://doi.org/10.1107/S0108768186098567
12. Palatnikov, M.N., Sidorov, N.V., Makarova, O.V., and Biryukova, I.V., *Fundamental'nye aspekty tekhnologii sil'no legirovannykh kristallov niobata litiya* (Fundamental Aspects of the Technology of Heavily Doped Lithium Niobate Crystals), Apatity: Kol'skii Nauchnyi Tsentr Ross. Akad. Nauk, 2017.
13. Palatnikov, M.N., Biryukova, I.V., Sidorov, N.V., Denisov, A.V., Kalinnikov, V.T., Smith, P.G.R., and Shur, V.Ya., Growth and concentration dependencies of rare-earth doped lithium niobate single crystals, *J. Cryst. Growth,* 2006, vol. 291, pp. 390–397.
https://doi.org/10.1016/j.jcrysgro.2006.03.022
14. Palatnikov, M.N., Masloboeva, S.M., Biryukova, I.V., Makarova, O.V., Sidorov, N.V., and Efremov, V.V., Effect of the method used to prepare solid precursors Nb_2O_5:Mg on the characteristics of $LiNbO_3$ crystals produced on their basis, *Russ. J. Inorg. Chem.,* 2014, vol. 59, no. 3, pp. 178–182.
https://doi.org/10.1134/S0036023614030176
15. Palatnikov, M.N., Birukova, I.V., Masloboeva, S.M., Makarova, O.V., Manukovskaya, D.V., and Sidorov, N.V., The search of homogeneity of $LiNbO_3$ crystals grown of charge with different genesis, *J. Cryst. Growth,* 2014, vol. 386, pp. 113–118.
https://doi.org/10.1016/j.jcrysgro.2013.09.038
16. Palatnikov, M.N., Biryukova, I.V., Masloboeva, S.M., Makarova, O.V., Kravchenko, O.E., Yanichev, A.A., and Sidorov, N.V., Structure and optical homogeneity of $LiNbO_3\langle Mg\rangle$ crystals grown from different charges, *Inorg. Mater.,* 2013, vol. 49, no. 7, pp. 715–720.
https://doi.org/10.1134/S0020168513060083
17. Palatnikov, M.N., Sidorov, N.V., Biryukova, I.V., Shcherbina, O.B., and Kalinnikov, V.T., Granulated starting mixture for the growth of lithium niobate single crystals, *Perspekt. Mater.,* 2011, no. 2, pp. 93–97.

Translated by O. Tsarev